Low-Profile Head-Worn Antenna with a Monopole-Like Radiation Pattern

Toni Björninen, *Member, IEEE*, Fan Yang, *Senior Member, IEEE*

***Abstract*—We present a low-profile antenna derived from a center-fed circular patch to provide uniform spatial coverage around a human head in 5.8 GHz ISM band. With the thickness of only 7 mm, it provides a compelling solution for a beacon-like radiator or harvester embedded in a smart headgear or in an in/off body communication relay-station. Below, we will first outline the development of an ellipsoid head model for numerically efficient optimization of the antenna and then detail the antenna development based on full-wave simulations. The results are validated using an anatomical head model and measurements both in air and in head-worn configuration. The measured results show that the antenna achieves a 0-dBi gain in the spatial angles around the head. The simulated radiation efficiency is 76% and SAR is well below ICNIRP and FCC limits even with 100 mW antenna power.**

***Index Terms*—Wearable antenna, patch-antenna, head-worn antenna, body area network, energy harvesting**

I. Introduction

WIRELESS body area networks (BAN) have become an increasingly important trend in the field of wireless communications during the past decade. The future development of wearable wireless technology will have an important role in the fields of safety and security, indoor localization and positioning, welfare and healthcare, and in bio-monitoring, for instance [1-3]. Overall, this development is striving toward wearable intelligence: the body-worn sensing and energy harvesting platforms will provide wireless power and data to the human intranet consisting of implanted and body-worn devices while an off-body communications unit connects it to the intelligent environment or internet the of things [4, 5].

The profound challenge in the optimization of wearable antennas is the mitigation of the negative impact arising from the electromagnetic (EM) interaction between the antenna and the dissipative biological tissue [6]. In the extremely cost-driven applications, such as radio-frequency identification, simple dipole antennas have been shown to provide detection range up to 3 with antenna-body separation of 3-to-4 mm [7]. Compared with a dipole, single-layer magnetic antennas based on slot-type radiators [6] have been shown to achieve generally better performance although they still suffer from the compromised radiation efficiency. In comparison, antennas with ground plane benefit from built-in antenna-body isolation. Here, several types of antennas have been studied, including fully textile-based microstrip patch antenna [8], IFA/PIFA [9-11], and antennas based on substrate-integrated waveguides and metamaterials [12-14]. However, they typically exhibit a directive radiation pattern and thus provide effective wireless communications only in specific off-body direction. As a remedy, body-worn arrays with high gain and steerable beam have been proposed [15, 16], but this comes with the cost of increased structural complexity.

As an alternative to the above-described solutions, we propose a low-profile antenna with a monopole-like radiation pattern for broad spatial coverage to enable reliable energy harvesting and off-body communications.

Manuscript received June 15, 2015; accepted August 20, 2015. Date of publication September 5, 2015; date of current version September 5, 2015. This research work was supported by the Academy of Finland (funding decision 265768).

Toni Björninen is with the Department of Electronics and Communications Engineering, Tampere University of Technology, Tampere, Finland (e-mail: toni@bjorninen@tut.fi).

Fan Yang is with the Microwave and Antenna Institute, Electronic Engineering Department, Tsinghua University, Beijing, China (e-mail: fan_yang@tsinghua.edu.cn).

II. Electromagnetic Models of the Human Head

In the EM modeling of the antenna, we used two different head models in ANSYS HFSS v.15 (a full-wave EM solver based on the finite element method). The ellipsoid model in Fig. 1 was created by fitting an ellipsoid to the head of the anatomical model of an adult male provided by ANSYS. The exterior surface is defined as a tri-axial ellipsoid with semi-axis lengths of 115.31 mm, 88.75 mm, and 77.44 mm, along the x'-, y'- and z'-axis in Fig. 1, respectively. The ellipsoid was truncated at z' = 70 mm to form a flat area for the

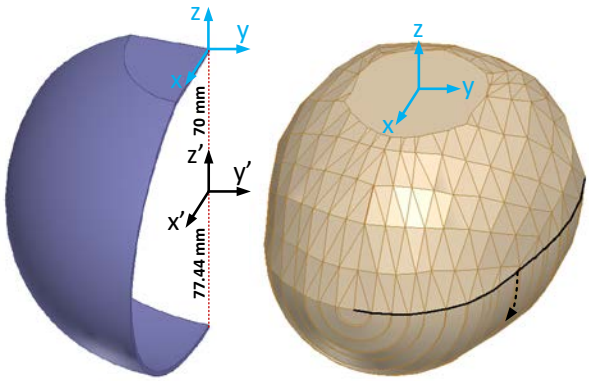

Fig. 1. Left: Ellipsoid model with symmetry boundaries at xz- and yz-planes. Right: model with anatomical shape in the upper hemisphere.

placement of the antenna. The truncation height was chosen maximal, so that it would produce minimal difference compared with the real head shape. Finally, the solid shape was reduced to a shell with the thickness of two millimeters and the dielectric properties of skin. The internal structure of the head was modelled by assigning a layered impedance boundary to the interior surface of the skin shell. This way, we combined the full-wave modeling of the antenna-body interactions in the skin layer and approximated the impact of the internal structure of the head based on an impedance boundary which represents the following layered structure: 2 mm of fat, 7 mm of cortical bone, 1 mm of cerebrospinal fluid (CSF), and 35 mm of grey brain matter. In the simulation, the dielectric properties of all of the biological tissues were based on the four-term Cole-Cole dispersion model with the parameters provided in [18]. Table I lists the dielectric properties of the tissues at 5.8 GHz. As a result, we have the complex impedance of $104.1+j50.7\ \Omega$ for the impedance boundary.

Thanks to the symmetric structure of our antenna (Section III) and the ellipsoid, we were able to employ the magnetic field symmetry boundary condition in HFSS to reduce the model size to a quarter of the full ellipsoid. This numerically efficient model was used in the antenna optimization. The optimization outcome was validated in a more detailed head model with an anatomical shape in the upper hemisphere. The shape is from ANSYS human body model, but in this work which is focused on off-body communications, we excluded the internal structure of the head such as brain and other tissue types and reduced it to a 2-mm shell of skin backed with the layered impedance boundary described above. Moreover, we considered the impact of the anatomical details in the lower hemisphere of the head negligible and created it by sweeping the equatorial line around its center axis as indicated in Fig. 1.

TABLE I
DIELECTRIC PROPERTIES OF BIOLOGICAL TISSUES USED IN THE HEAD MODELS AT 5.8 GHZ

	Skin	Fat	Bone, cortical	CSF	Brain, grey matter
ε_r	35.11	9.86	9.67	60.47	44.00
tanδ	0.33	0.26	0.37	0.40	0.35

III. ANTENNA STRUCTURE AND SIMULATED RESULTS

We commenced the antenna development based on a center-fed circular microstrip patch antenna. In free-space, it radiates similar to a monopole with a broadside null and uniform radiation pattern in the antenna plane [17]. The polarization of the antenna is linear with the electric field vector orthogonal to the antenna plane. As a constraint for the size of the antenna, we considered the relatively flat area on top of the head. The conductor areas of the antenna were pattern from copper tape which was adhered on soft and conformal EPDM (Ethylene-Propylene-Diene-Monomer) foam. The dielectric properties of $\varepsilon_r = 1.3$ and $\tan\delta = 0.0015$ were measured for the EPDM at 5.8 GHz using Agilent 85070E dielectric probe. However, since this method is suited best for the measurement of liquids, we must consider the obtained values only indicative.

Because the circularly symmetrical structure of the antenna is essential for achieving the uniform radiation pattern, we considered the coaxial probe feed the best approach for feeding the antenna. However, here the challenge was that even though the ground plane provides built-in antenna-body isolation, it would be cumbersome to place cables and connectors between the head and the ground plane. Hence, our approach was to face the ground plane away from the head and to insert another conductor layer between the head and the patch to provide electromagnetic isolation. This way, the antenna is fed from the top which provides a natural way of using the backside of the ground plane as a platform for additional electronics in communications and harvesting systems based on the proposed antenna.

The asymmetric shape of the head influences the antenna radiation. We found that in order to achieve uniform radiation pattern in the head-worn configuration, it was best to replace the disk-shaped antenna with an ellipsis with the major axis along the longer dimension of the head (x-axis in Fig. 1). However, we observed that at 5.8 GHz the most uniform radiation patterns tended to be produced by structures with a resonance frequency around 5.5 GHz. As a remedy, we introduced four shorting pins around the feed probe. By inserting them at different distances from the probe along the major and minor axes of the ellipsis, we achieved an additional degree of freedom in optimization of the radiation pattern. After establishing the antenna structure shown in Fig. 2 as a feasible candidate, we optimized the parameters r, k, u, and v in the ellipsoid head model using the built-in genetic algorithm in HFSS. In order to simultaneously maximize the radiation efficiency (e_r), minimize the input reflection coefficient ($|s_{11}|^2$) and maximize and uniformize the antenna directivity (D) in the xy-plane, the target in the optimization

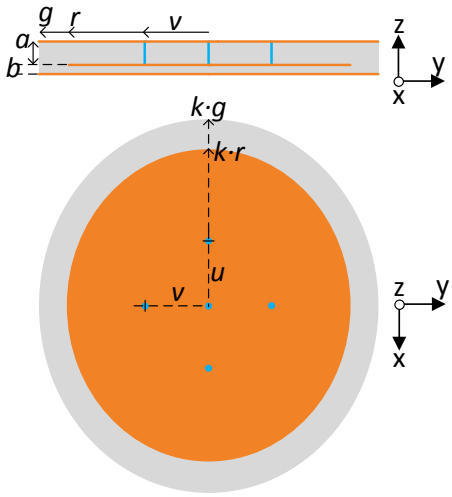

	a	b	r	g	k	u	v
A1	5	2	32.5	36.5	1.1	13	13.5
A2	5	2	30.5	36.5	1.1	14	13.5

Fig. 2. Structure of the antenna and the dimensions of prototypes A1 and A2 in millimeters. The coordinate system is the same as in Fig. 1.

TABLE II
SIMULATED PERFORMANCE OF ANTENNAS A1 AND A2 AT 5.8 GHZ IN THE TWO DIFFERENT HEAD MODELS

	Ellipsoid		Anatomical	
	A1	A2	A1	A2
$\lvert s_{11}\rvert^2$ [dB]	−12.8	−38.9	−12.4	−30.8
e_r	0.76	0.76	0.77	0.77
$\min_\phi D(90^\circ,\phi)$ [dBi]	0.52	0.37	−0.04	−0.24
$\min_\phi G_r(90^\circ,\phi)$ [dBi]	−0.85	−0.80	−1.40	−1.37

TABLE III
SIMULATED MAXIMUM AVERAGE SAR AND THE MAXIMUM SAR-COMPLIANT POWER IN THE ANTENNA AT 5.8 GHZ

	A1 ICNIRP	A2 ICNIRP	A1 FCC	A2 FCC
SAR [W/kg] with P_{ant} = 0.1W	0.100	0.098	0.271	0.266
$P_{ant,max}$ [W]	2.000	2.043	0.592	0.601

process was to maximize the minimum of the realized gain (G_r) given by $G_r = e_r(1-|s_{11}|^2)D$ in the xy-plane in Fig. 1.

From the total of 600 optimizer iterations, we selected two promising realizations. Henceforth, they are referred to as A1 and A2. The simulated performance of the antennas in both head models is summarized in Table II. A1 achieved the most uniform pattern (although just marginally better compared with A2), whereas A2 provided excellent matching at the center frequency. The simulated $|s_{11}|^2$ and e_r was virtually the same in both head models. The main difference between the predictions of the two models is that the anatomical model predicted approximately 0.5 dB lower $\min_\phi D(90°,\phi)$ for both antennas. The simulated input reflection coefficient versus frequency and antenna gain patterns at 5.8 GHz in air and in head-worn configurations will be presented along with the measured results in the next section.

To clarify the importance of the isolator layer and ellipsis-versus-circle shape, we report below the performance data for A1 in two cases: with the isolator removed and with the antenna shape changed to a disk with the radius equal to the minor semi-axis of the ellipsis. Removal of the isolator resulted in e_r = 0.52 and $\min_\phi D(90°,\phi)$ = −0.1 dBi in the anatomical model, whereas the disk-shaped antenna lead to e_r = 0.76 and $\min_\phi D(90°,\phi)$ = −0.87 dBi. Hence, the isolator improves e_r as much as 24 %-points and the ellipsis shape brings an improvement of 0.83 dB in $\min_\phi D(90°,\phi)$.

Finally, we simulated the maximum average specific absorption rate (SAR) considering both ICNIRP and FCC limits of 2 W/kg and 1.6 W/kg averaged over 10 g and 1 g of tissue, respectively. In both cases the averaging cube overlaps several tissue types with different dielectric properties and densities. Therefore, to ensure numerical stability and reproducibility of the data, we considered a simplified model consisting of $15\times15\times5$ cm^3 block of skin. Here, skin was selected as the tissue type, since in practice the highest local SAR occurs on its surface. As in reality the curvature of the head is expected to reduce the electromagnetic antenna-body interaction away from the antenna edges, we considered this worst-case estimation. Overall, the SAR values in Table III are low and, for instance, with 100 mW antenna power (P_{ant}), the exposure is lower than from modern cell phones. The maximum SAR-compliant antenna power of $P_{ant,max}$ = 2 W is much higher than typically used in body-worn mobile units. In ambient energy harvesting, the SAR values will be orders of magnitude lower.

IV. MEASURED RESULTS

The studied antennas were tested both in air and in head-worn configuration. Firstly, the input reflection coefficient was measured using vector network analyzer with the antenna in air and when placed on a subject's head. As seen from Fig. 3, the measured and simulated result for A1 in air agree closely. This confirms the successful simulation and construction of the antenna. In the head-worn configuration, there is a difference of approximately 80 MHz between the measured and simulated matched frequency. This can be attributed to the somewhat higher uncertainty in this measurement. Similar conclusions are drawn from Fig. 6 for A2, but in this case the agreement of the simulation and measurement is very close also in the head-worn configuration. The results show also that A1 and A2 achieve the measured impedance bandwidths ($|s_{11}|^2 < -10$ dB) of 330 MHz and 370 MHz, respectively, which is more than enough to cover the world wide ISM band from 5.725 to 5.875 GHz.

The gain patterns were measured in a far-field range. The data in air was recorded with the steps of 3° and averaged over 20 repetitions. In the head-worn configuration, steps of 6° and averaging over 8 repetitions were used. The measured and simulated results in air (Figs. 4 and 7) are in good agreement and predict close to 0 dBi gain in all directions. In the head-worn configuration, the antenna was attached to a block foam suspended on the measurement system holders with the antenna facing downward. The cable was inserted vertically through the foam. The subject was sitting below the antenna on a chair with the height adjusted to press the antenna tightly on his head. Due to the unintentional movements of the subject during the measurement, the uncertainty is higher than in the measurement in air. Also, the simulation model is for a specific head anatomy and does not include the impact of hair. For antenna A1, the measured gain (Fig. 5) fluctuates evenly on both sides of the simulation result, but on average we consider these results to be in a good agreement. For antenna A2, the measured gain (Fig. 8) in the directions of ±50° and ±135° is slightly lower compared with the simulation. However, also in this case the results are in fair agreement.

V. CONCLUSIONS AND FUTURE WORK

Reliable energy harvesting and off-body communication in body-area networks prompt the need for low-profile antennas with broad spatial coverage. We demonstrated that a center-fed ellipsis-shaped patch antenna achieves a monopole-like radiation pattern covering the spatial directions around the human head with a constant 0-dBi gain at 5.8 GHz. The antenna has the thickness of only 7 mm and it is fed from the top to avoid insertion of cables between the antenna and head. A layer of conductor acting as an isolator between the patch and the biological tissue enabled the high radiation efficiency

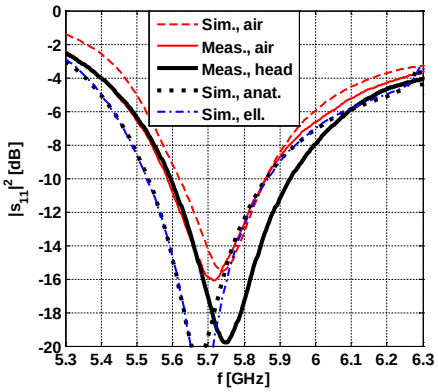

Fig. 3. Input reflection coefficient of A1.

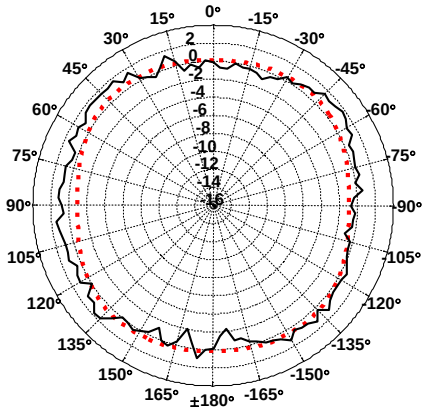

Fig. 4. Measured and simulated gain [dBi] of A1 in air in the xy-plane of Fig. 2 (0° towards the positive x-axis). Measured = solid line, simulated = dotted line.

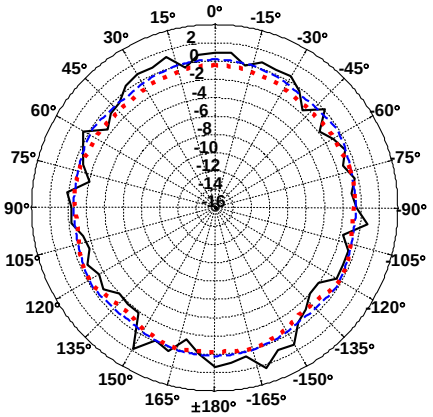

Fig. 5. Measured and simulated gain [dBi] of A1 on head in the xy-plane of Fig. 1 (0° towards the pos. x-axis). Measured = solid line, ellipsoid model = dashed line, anatomical model = dotted line.

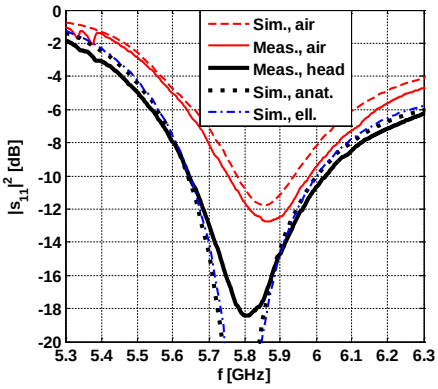

Fig. 6. Input reflection coefficient of A2.

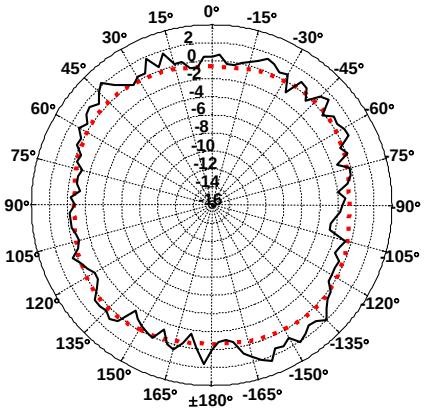

Fig. 7. Measured and simulated gain [dBi] of A2 in air in the xy-plane of Fig. 2 (0° towards the positive x-axis). Measured = solid line, simulated = dotted line.

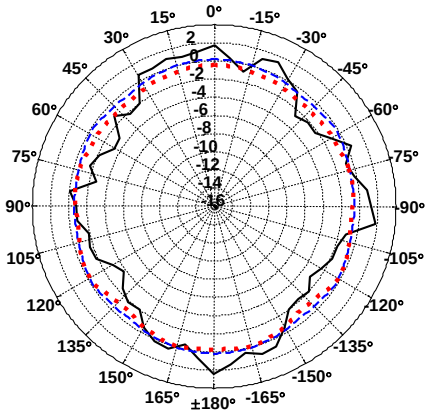

Fig. 8. Measured and simulated gain [dBi] of A2 on head in the xy-plane of Fig. 1 (0° towards the pos. x-axis). Measured = solid line, ellipsoid model = dashed line, anatomical model = dotted line.

of 76%. Future work includes the investigation of periodic loadings for on-body communication through surface waves and integration of an inductive loop in the isolator layer to form an integrated in/on/off-body communications platform.

REFERENCES

[1] Ya-Li Zheng, Xiao-Rong Ding, C. C. Y. Poon, B. P. L. Lo, Heye Zhang, Xiao-Lin Zhou, Guang-Zhong Yang, Ni Zhao, Yuan-Ting Zhang, "Unobtrusive sensing and wearable devices for health informatics," *IEEE Trans. Biomed. Eng.*, vol. 61, no. 5, pp. 1538–1554, May 2014.

[2] S. Movassaghi, M. Abolhasan, J. Lipman, D. Smith, A. Jamalipour, "Wireless body area networks: a survey," *IEEE Communications Surveys & Tutorials*, vol. 16, no. 3, pp. 1658–1686, Third Quarter 2014.

[3] Hoi-Jun Yoo, "Your heart on your sleeve: advances in textile-based electronics are weaving computers right into the clothes we wear," *IEEE Solid-State Circuits Mag.*, vol. 5, no. 1, pp. 59–70, winter 2013.

[4] J. M. Rabaey, "The human intranet—where swarms and humans meet," *IEEE Pervasive Comput.*, vol. 14, no. 1, pp. 78–83, Jan.–Mar. 2015.

[5] S. Lemey, F. Declercq, H. Rogier, "Textile antennas as hybrid energy-harvesting platforms," *Proc. IEEE*, vol. 102, no. 11, pp. 1833–1857, Nov. 2014.

[6] R. M. Mäkinen, T. Kellomäki, "Body effects on thin single-layer slot, self-complementary, and wire antennas," *IEEE Trans. Antennas Propag.*, vol. 62, no. 1, pp. 385–392, Jan. 2014.

[7] T. Björninen, J. Virkki, L. Sydänheimo, L. Ukkonen, "Impact of recurrent stretching on the performance of electro-textile UHF RFID tags," in ESTC, Sep. 2014, Helsinki, Finland, 5 p.

[8] P. B. Samal, P. J. Soh, G. A. E. Vandenbosch, "UWB all-textile antenna with full ground plane for off-body WBAN communication," *IEEE Trans. Antennas Propag.*, vol. 62, no. 1, Jan. 2014, pp. 102–108.

[9] Shengjian J. Chen, T. Kaufmann, C. Fumeaux, "Shorting strategies for a wearable L-slot planar inverted-F antenna," iWAT, March 2014, pp. 18–21.

[10] W. El Hajj, C. Person, J. Wiart, "A novel investigation of a broadband integrated inverted-F antenna design; application for wearable antenna," *IEEE Trans. Antennas and Propag.*, vol. 62, no. 7, pp. 3843–3846, July 2014.

[11] P. J. Soh, G. A. E. Vandenbosch, S. L. Ooi, M. R. N. Husna, "Design of a broadband all-textile slotted PIFA," *IEEE Trans. Antennas. Propag.*, vol. 60, no. 1, pp. 379-384, Jan. 2012.

[12] Shaozhen Zhu, R. Langley, "Dual-band wearable textile antenna on an EBG substrate," *IEEE Trans. Antennas Propag.*, vol. 57, no. 4, pp. 926–935, Apr. 2009.

[13] H. R. Raad, A. I. Abbosh, H. M. Al-Rizzo, D. G. Rucker "Flexible and compact AMC based antenna for telemedicine applications," *IEEE Trans. Antennas Propag.*, vol. 61, no. 2, pp. 524–531, Feb. 2013.

[14] S. Agneessens, S. Lemey, T. Vervust, H. Rogier, "Wearable, small, and robust: the circular quarter-mode textile antenna," *IEEE Antennas Wireless Propag. Lett.*, 2015.

[15] M. L. Scarpello, L. Vallozzi, H. Rogier, D. Vande Ginste, "High-gain textile antenna array system for off-body communication," *Intl. J. Antennas Propag.*, vol. 2012, Article ID 573438, 12 p.

[16] Seonghun Kang, Chang Won Jung, "Wearable fabric reconfigurable beam-steering antenna for on/off-body communication system," *Intl. J. Antennas Propag.*, vol. 2015, Article ID 539843, 7 p.

[17] F. Yang, Y. Rahmat-Samii, A. Kishk, "Low-profile patch-fed surface wave antenna with a monopole-like radiation pattern," *IET Microw. Antennas Propag.*, no. 1, vol. 1, Feb. 2007.

[18] S. Gabriel, R. W. Lau, C. Gabriel, "The dielectric properties of biological tissues: III. Parametric models for the dielectric spectrum of tissues," *Phys. Med. Biol.*, vol. 41, no. 11., pp. 2271–2293, Nov. 1996.